Electronic Supplementary Material (ESI) for Chemical Communications.
This journal is © The Royal Society of Chemistry 2021

SUPPORTING INFORMATION

Supporting Information

A vacancy-rich perovskite fluoride $K_{0.79}Ni_{0.25}Co_{0.36}Mn_{0.39}F_{2.83}$@rGO anode for advanced Na-based dual-ion batteries

Caini Tan[a], Rui Ding*[a], Yuxi Huang [a], Tong Yan[a], Yongfa Huang[a], Feng Yang[a], Xiujuan Sun[a], Ping Gao[a], and Enhui Liu[a]

[a] Key Laboratory of Environmentally Friendly Chemistry and Applications of Ministry of Education, College of Chemistry, Xiangtan University, Xiangtan, Hunan 411105, P.R. China

*Corresponding Author

*E-mails: drm8122@163.com; drm8122@xtu.edu.cn

Supporting Information

Synthesis of KNCMF@rGO materials

Analytical/guaranteed reagents (AR/GR) were directly used in the experiment (**Table S1)**. The KNCMF@rGO(Ni:Co:Mn=1:1:1) sample was synthesized via a facile one-pot solvothermal route. Firstly, 60 mg graphene oxides (GO) powder was dispersed in 32 mL ethylene glycol (EG) solvents with an ultrasonic bath for 2 h at 100 W. Secondly, 0.66 mmol $NiCl_2$•$6H_2O$, 0.66 mmol $CoCl_2$•$6H_2O$, 0.66 mmol $MnCl_2$•$4H_2O$, 5 mmol KF•$2H_2O$, and 0.20 g PVP-K30 were dissolved into GO solution, and then the mixture was magnetically stirred thoroughly and dispersed well in an ultrasonic bath for 30 min at 100 W. Thirdly, the mixture was transferred into a 50 mL Teflon-lined stainless steel autoclave, which was heated at 180 ℃ for 12 h in an electric oven, and then cooled down naturally. Next, the yielded precipitates were collected after being centrifuged along with absolute alcohol washing for several times. Finally, the precipitates were dried overnight at 95 ℃ to obtain the products. The synthesis procedure of KNMF@rGO(Ni: Mn=1: 1), KCMF@rGO(Co:Mn=1:1), KNCF@rGO(Ni:Co =1:1), KNiF@rGO, KCoF@rGO and KMnF@rGO are the same as KNCMF@rGO(Ni:Co:Mn=1:1:1) except for the molar ratio of Ni, Co, and Mn slats.

Characterizations

The phases and crystallinity properties were determined by X-ray diffraction (XRD). The morphology and size of particles were analyzed by scanning electron microscopy (SEM) and transmission electron microscopy (TEM). The crystalline microstructures were resolved by the high-resolution TEM (HRTEM) and selected area electron diffraction (SAED). The element composition and distribution were measured by the X-ray energy dispersive spectra (EDS), inductively coupled plasma-optical emission spectrometer (ICP-OES) and mapping. The surface chemical compositions and electronic structures were checked by X-ray photoelectron spectra (XPS). The specific surface area, pore volume and size distribution were examined by nitrogen isothermal sorptions with Brunauer-Emmett-Teller (BET) and Barrett-Joyner-Halenda (BJH) methods. The existence and content of reduction graphene oxide were analyzed by

Thermogravimetric analysis (TG) and di□erential Thermogravimetric (DTG).

Electrochemical measurements

The electrodes were prepared by the following two steps: firstly, a well-dispersed mixture of 70 wt% active materials, 10 wt% acetylene black (AB) conductive agent/10 wt% superconductive carbon black (for KNCMF@rGO electrode while 20 wt% superconductive carbon for KS6 electrode, respectively), and 10 wt% polyvinylidene fluoride binder (PVDF, which was dissolved in N-methyl-2-pyrrolidone (NMP)). The KNCMF@rGO and KS6 paste was respectively cast onto the current collectors of Cu foil as the anode and carbon-coated Al foil as the cathode, followed by drying in a vacuum oven at 110 ℃ for 12 h; secondly, the electrodes were punched into disks with a diameter of 12 mm, and the mass loading of active materials was about 1-2 mg cm^{-2}. The electrolytes used for KNCMF@rGO, KS6 electrodes, and Na-DIBs were 0.85 M $NaPF_6$ dissolved in the mixed solvents of ethylene carbonate (EC), ethyl methyl carbonate (EMC) and diethyl carbonate (DEC) (1 : 1 : 1 in volume) with 5 % fluoroethylene carbonate (FEC) additive (Na206-181224, MJS); all cell assemblies were performed in a high pure Ar-filled dry glovebox (MIKROUNA, O_2 and H_2O < 0.1 ppm) and all tests were carried out at room temperature (about 25 ℃) except the assigned tests at high (40 ℃) and low (-20 ℃) temperatures (more detailed information about the above mentioned chemicals, agents, and materials can be seen in **Table S1**.). We used the same cell to test the specific capacity at 0.02-1-0.02 A g^{-1} and cycling at 0.3 A g^{-1} for 500 cycles (before testing the cycling the cell was laid aside for 3 hours) of KNCMF@rGO electrode. Furthermore, we used a new cell to test the cycling (0.5 A g^{-1}/500 cycles) of the KNCMF@rGO, KNMF@rGO, KNCF@rGO, KCMF@rGO, KNF@rGO, KCF@rGO and KMF@rGO electrodes.

Calculations for C_m, E_m, P_m

The specific capacity (C_m, mAh g^{-1}), energy density (E_m, Wh kg^{-1}), and power density (P_m, kW kg^{-1}) for Na-DIBs were calculated according to the **Equations S(1)-S(3)**.

$$C_m = Q_m / 3.6 \quad \text{S(1)}$$

$$E_m = \int_0^{C_m} V dC_m \quad \text{S(2)}$$

$$P_m = 3.6\, E_m / t_d \quad \text{S(3)}$$

Where m, Q_m, V and t_d refer to the mass of active materials (mg, for half cells, it means the mass of active materials of anode or cathode; for Na-DIBs full cells, it means the total mass of active materials of anode and cathode), specific charge or discharge quantity (C g^{-1}, for anode, it means the charge quantity; for cathode and full cells, it refers to the discharging quantity), Voltage (V), and discharging time (s) , respectively.

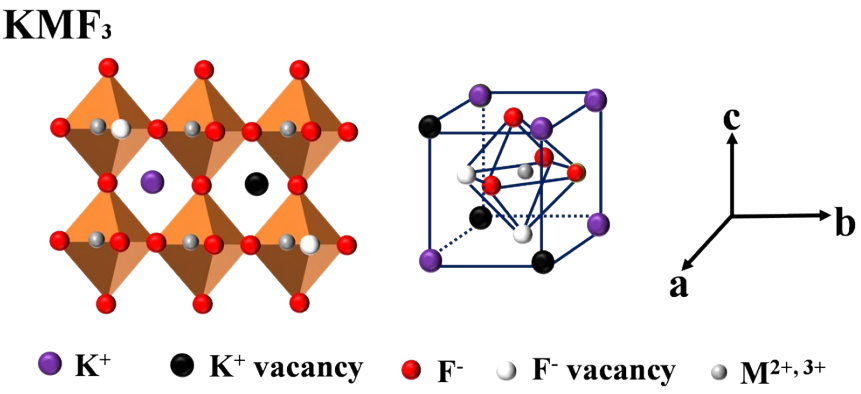

Sample	ICSD-PDF	Crystal system	Space group	Cell (a×b×c)/Å^3
$KNiF_3$	21-1002	Cubic	*Pm-3m*	4.0127×4.0127×4.0127
$KCoF_3$	18-1006	Cubic	*Pm-3m*	4.0708×4.0708×4.0708
$KMnF_3$	17-0116	Cubic	*Pm-3m*	4.1890×4.1890×4.1890

Figure S1. The crystal structures of perovskite KMF_3 and detailed crystalline parameters for $KNiF_3$, $KCoF_3$, and $KMnF_3$.

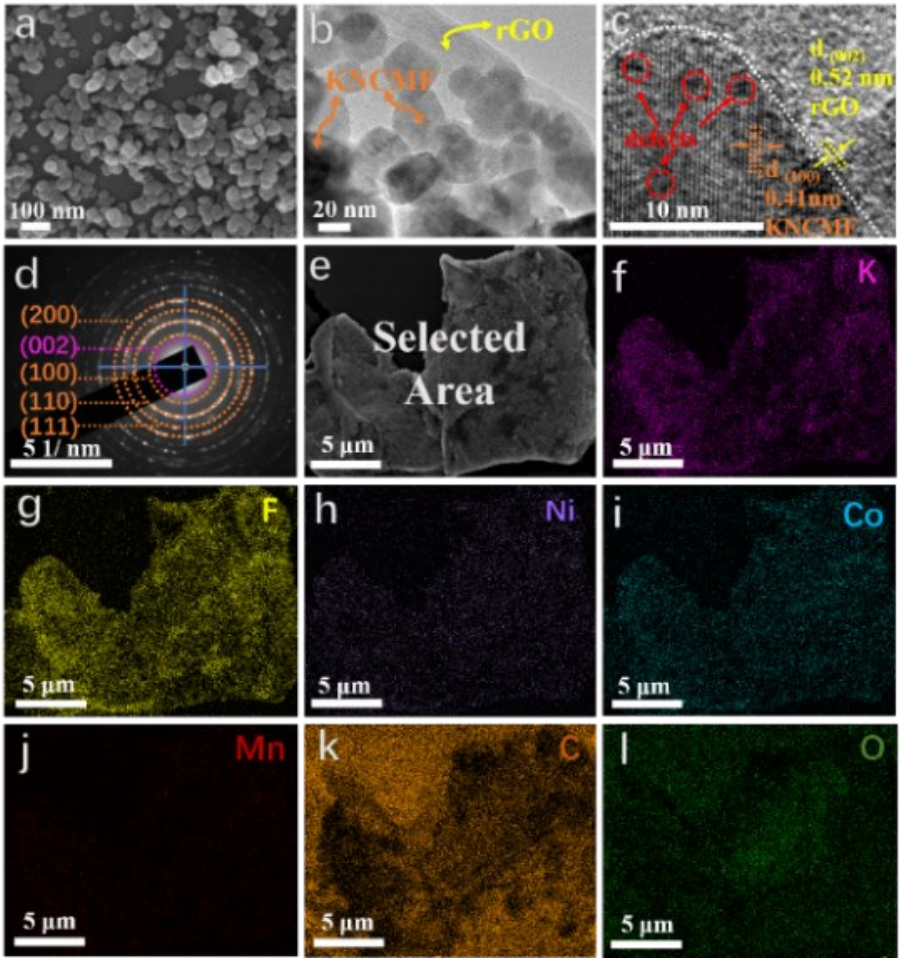

Figure S2. SEM (a), TEM (b), HRTEM (c), SAED(d), mapping (e-l) of the KNCMF@rGO candidate.

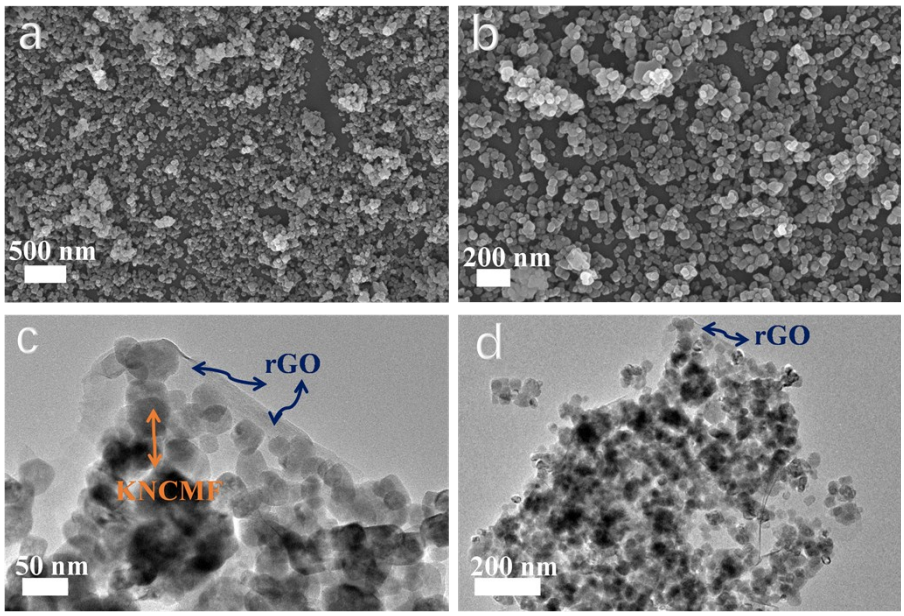

Figure S3. SEM and TEM images of the KNCMF@rGO Sample.

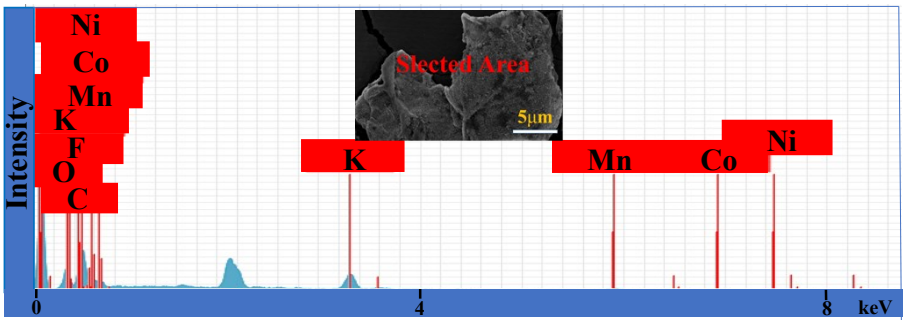

Figure S4. EDS of the KNCMF@rGO Sample.

Result from ICP-OES	
Element	**Wt.%**
K	21.79
Ni	10.36
Co	14.87
Mn	15.27
Formula	$K_{0.79}Ni_{0.25}Co_{0.36}Mn_{0.39}F_{2.83}$

Figure S5. ICP of the KNCMF@rGO Sample.

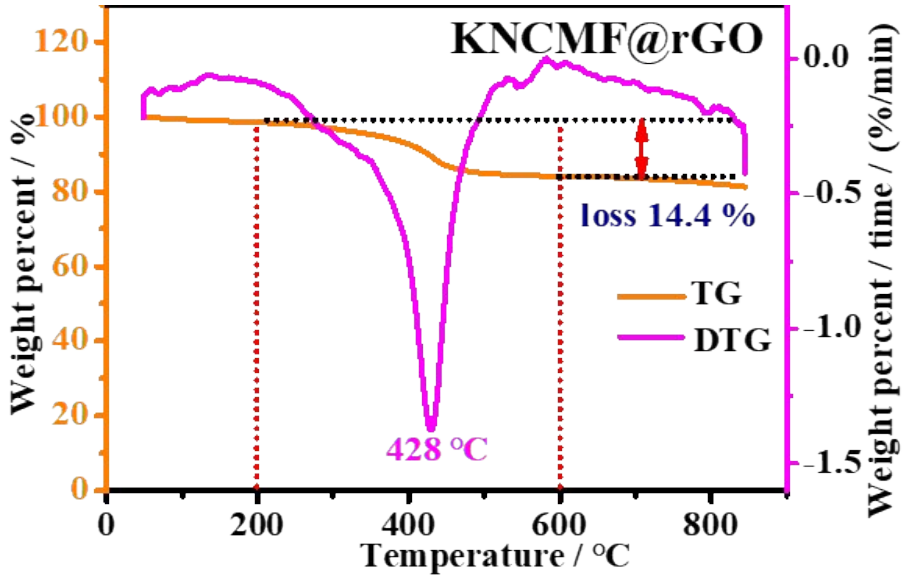

Figure S6. TG/DTG curves of the KNCMF@rGO Sample.

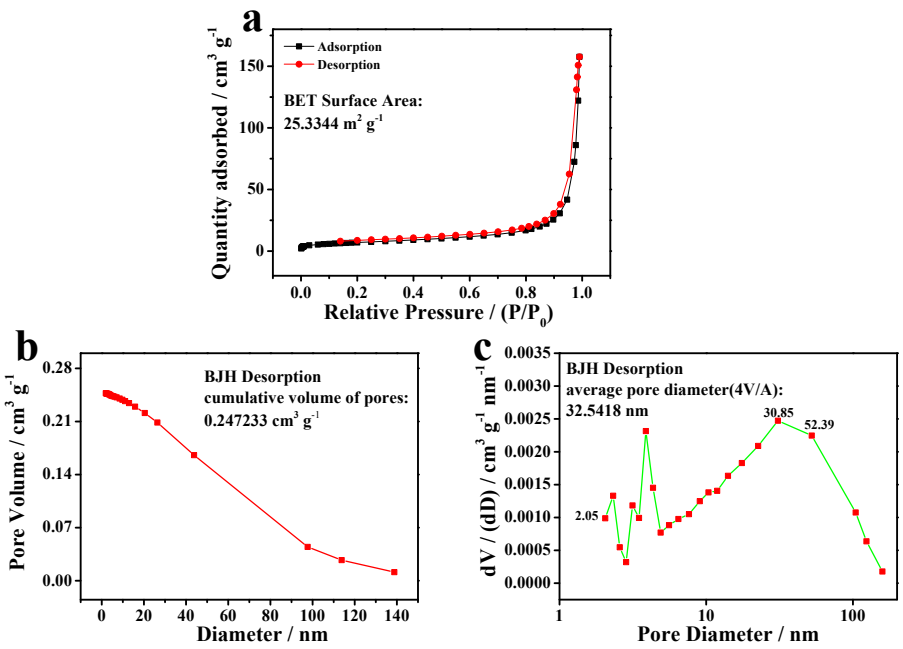

Figure S7. N_2 isothermal sorptions (a), pore volumes (b), and pore size distributions (c) of the KNCMF@rGO Sample.

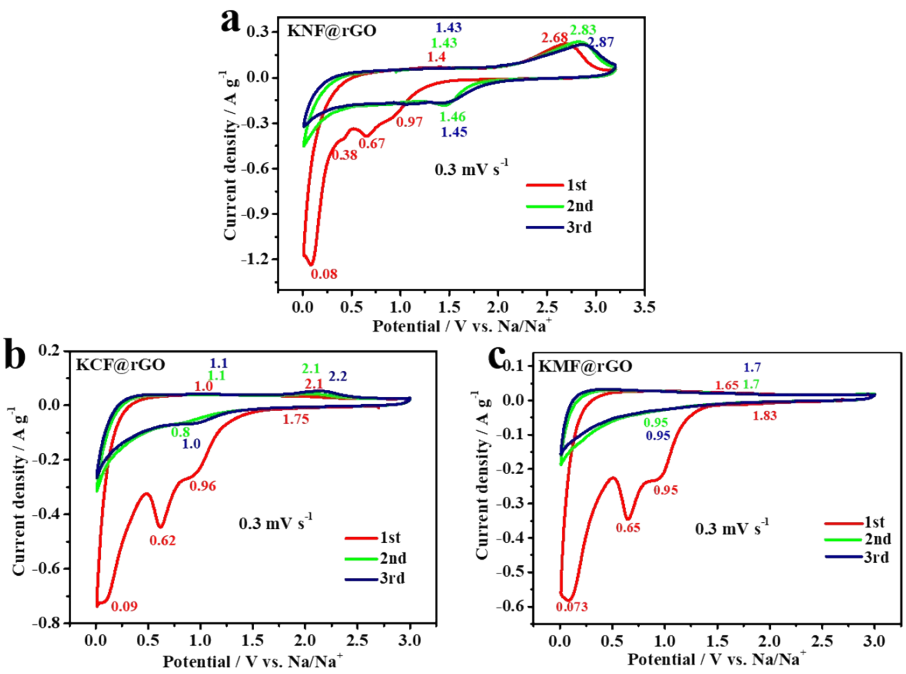

Figure S8. CV plots for the first three cycles at 0.3 mV s^{-1} of KNF@rGO electrode (a); KCF@rGO electrode (b); and KMF@rGO electrode (c).

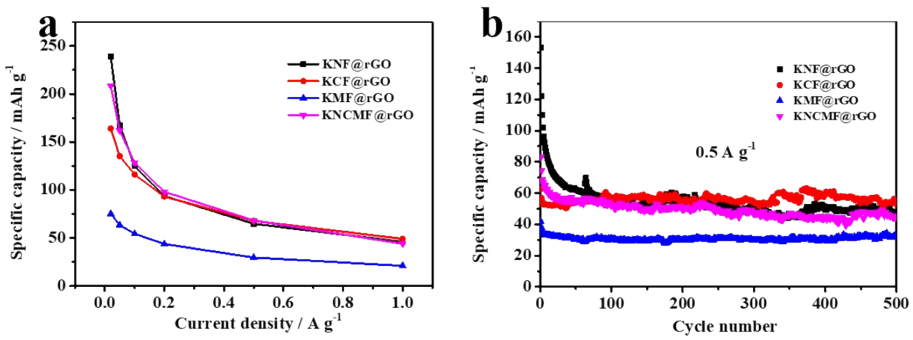

Figure S9. Specific capacity (a) and cycling stability (b) of KNF@rGO, KCF@rGO, KMF@rGO, and KNCMF@rGO electrode.

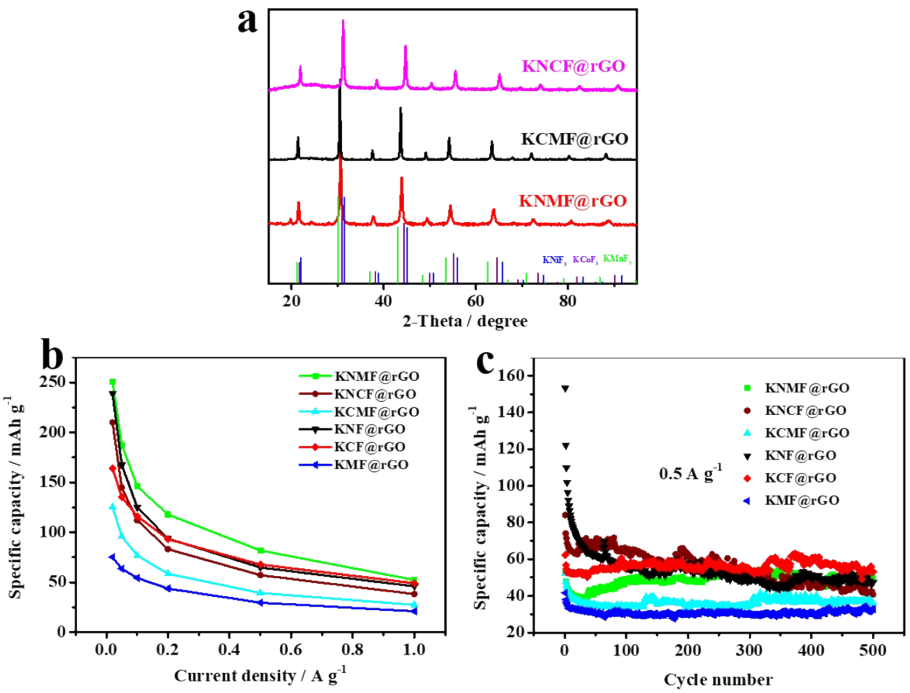

Figure S10. XRD patterns of KNCF@rGO, KCMF@rGO and KNMF@rGO samples (a), specific capacity (b) and cycling stability (c) of KNMF@rGO, KNCF@rGO, KCMF@rGO, KNF@rGO, KCF@rGO and KMF@rGO electrodes.

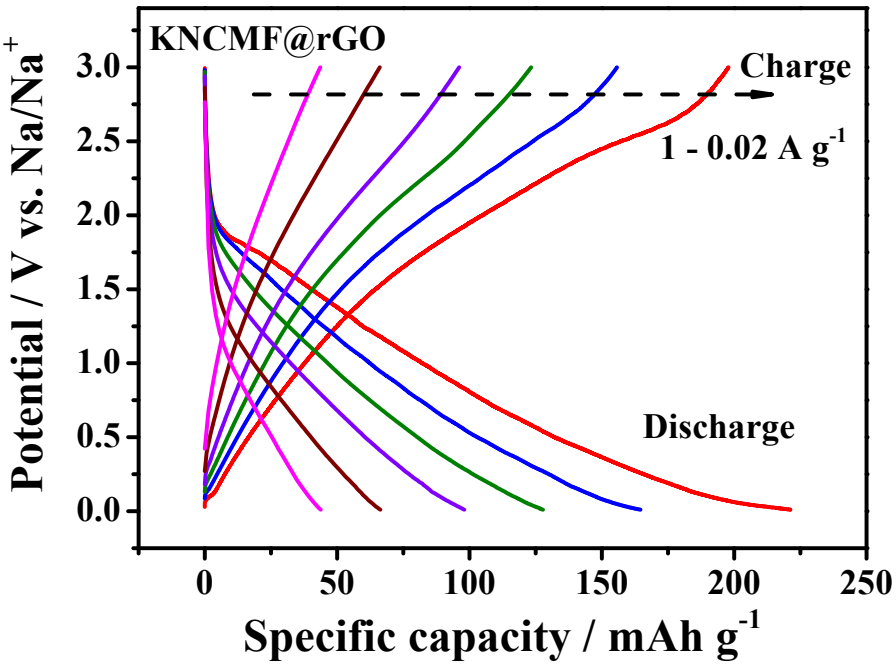

Figure S11. GCD curves of the KNCMF@rGO electrode.

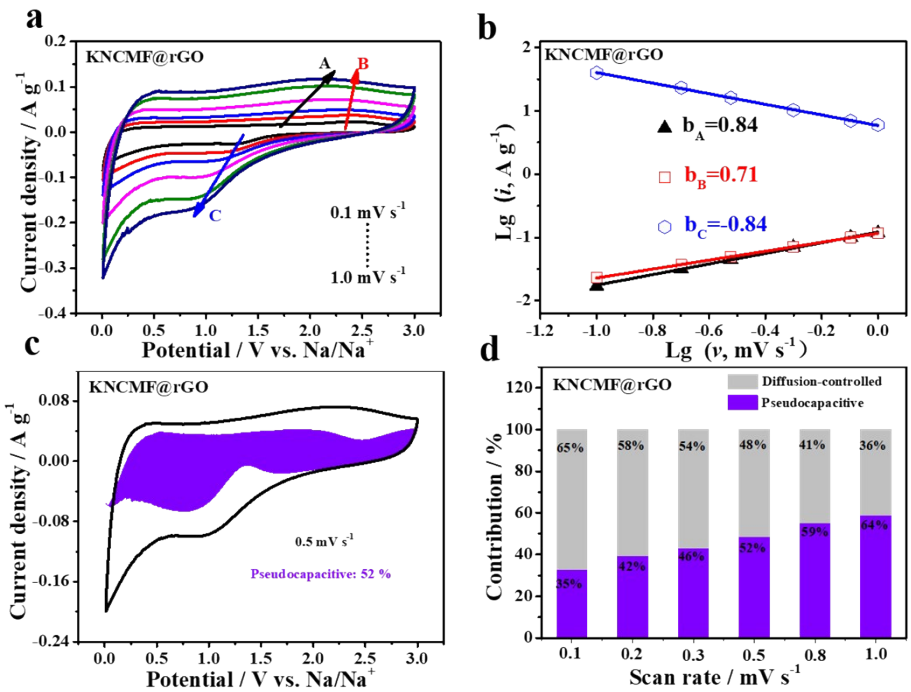

Figure S12. CV plots at 0.1-1.0 mV s^{-1}(a); plots of lg*i* vs.lg*v* (b); the pseudocapacitive contribution at a scan rate of 0.5 mV s^{-1} (c); and charge contributions by the diffusion-controlled and pseudodcapacitive contribution at different scan rates (d) of the KNCMF@rGO electrode.

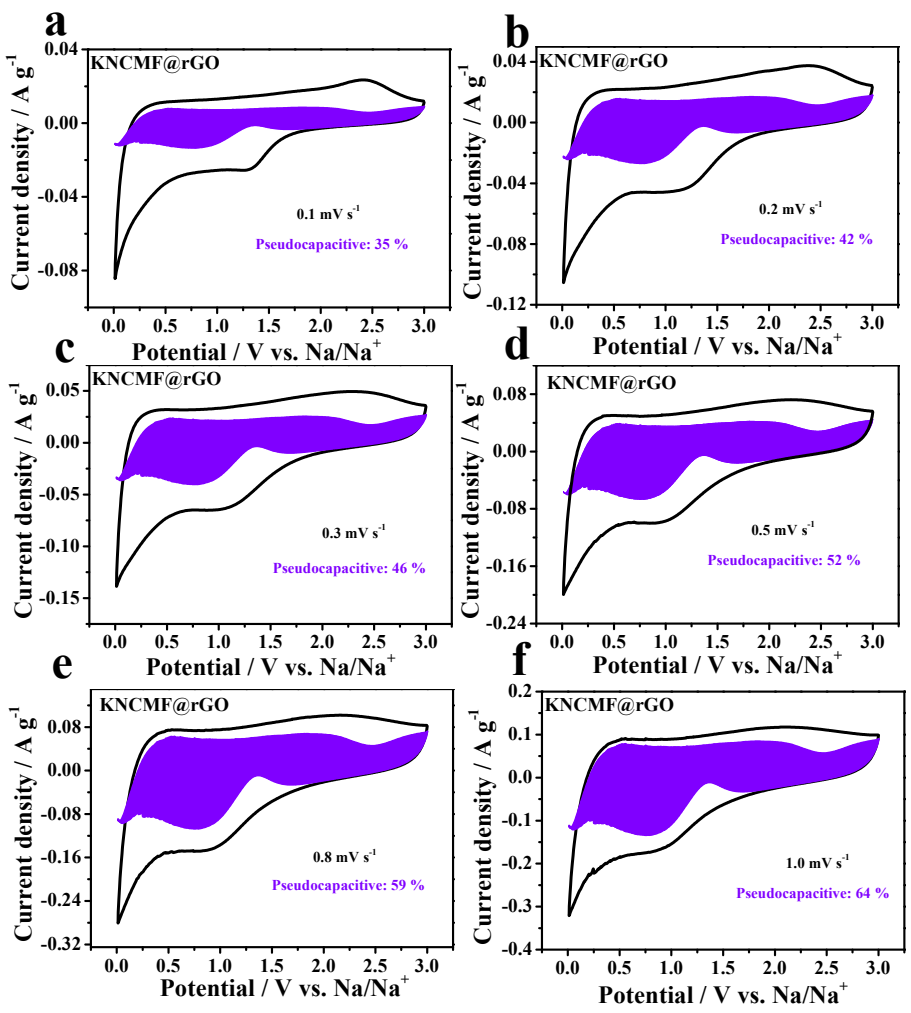

Figure S13. Pseudocapacitive contribution map at 0.1-1.0 mV s^{-1} (a)-(f).

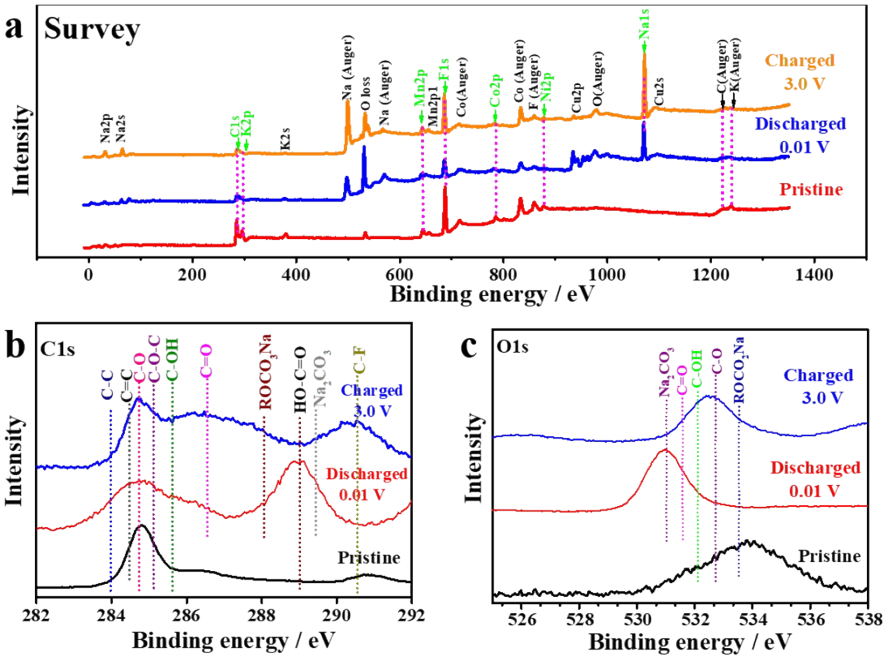

Figure S14. Ex-situ XPS spectra of the KNCMF@rGO electrode in pristine, discharged-0.01 V and charged-3.0 V states during the first discharged/charged cycle at 0.02 A g^{-1}: survey (a), C1s (b) and O1s (c).

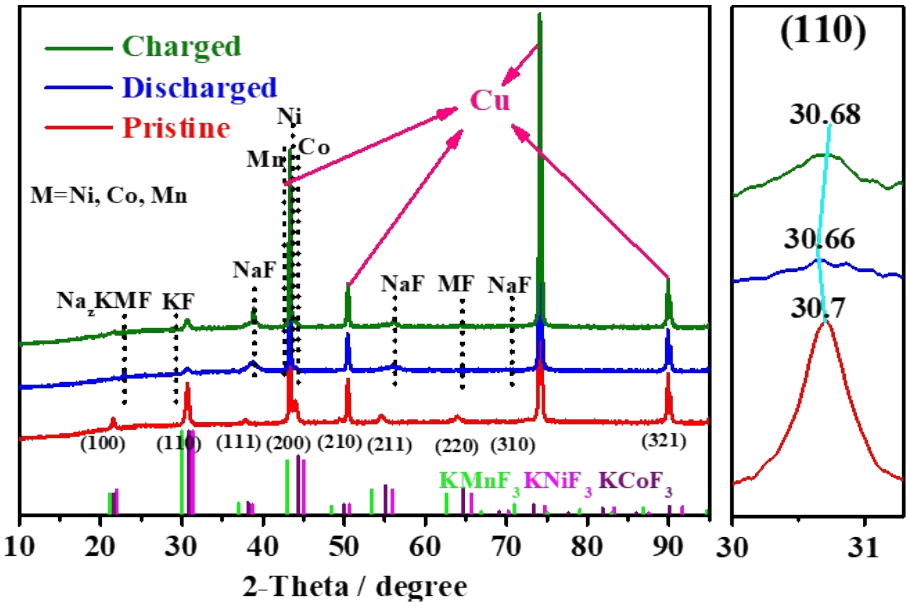

Figure S15. Ex-situ XRD in pristine and first fully discharged/charged states of the KNCMF@rGO electrode.

(a)

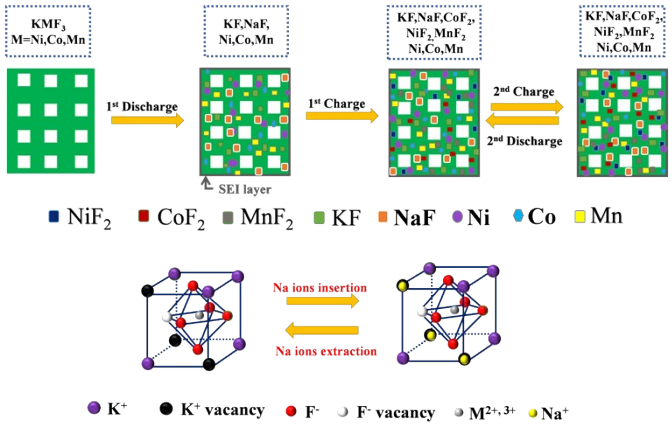

（b）

Phases	PDF Card	Crystal system	Space group	Cell (a×b×c)/Å^3
Ni	**45-1027**	**Hexagonal**	**P63/mmc**	**2.6515×2.6515×4.343**
Co	**05-0727**	**Hexagonal**	**P63/mmc**	**2.5031×2.5031×4.0605**
Mn	**17-0910**	**Tetragonal**	**I4/mmm**	**2.672×2.672×3.55**
NiF_2	**22-0749**	**Orthorhombic**	**P42/mnm**	**4.56×4.77×3.065**
CoF_2	**38-0883**	**Cubic**	**Pa-3**	**4.958×4.958×4.958**
MnF_2	**34-1326**	**Tetragonal**	**P-42m**	**5.112×5.112×5.256**
NaF	**36-1455**	**Cubic**	**Fm-3m**	**4.63329×4.63329×4.63329**
KF	**36-1458**	**Cubic**	**Fm-3m**	**5.34758×5.34758×5.34758**
Na_2CO_3	**25-0815**	**Hexagonal**	**P63/mc**	**5.215×5.215×6.584**

（c）

$$x K_{0.79}MF_{2.83} + 2.04x Na^+ + 2.04x e^- \rightarrow xM + 0.79x KF + 2.04x NaF \quad (1)$$

$$yM + 2yNaF \leftrightarrow yMF_2 + 2yNa^+ + 2ye^- \quad (2)$$

$$K_{0.79}M(\text{Ⅱ})_{0.96}M(\text{Ⅲ})_{0.04}F_{2.83} + zNa^+ + ze^- \leftrightarrow Na_zK_{0.79}M(\text{Ⅱ})_{0.96+z}M(\text{Ⅲ})_{0.04-z}F_{2.83} \quad (3)$$

$$qNa^+ + qe^- + xM/2.04xNaF \leftrightarrow xM/qNa/2.04xNaF \quad (4)$$

$$rNa^+ + re^- + xM/2.04xNaF \leftrightarrow rNa/xM/2.04xNaF \quad (5)$$

$$nC + mNa^+ + me^- \leftrightarrow Na_mC_n \quad (6)$$

$$Na^+ + \text{electrolytes} + e^- \leftrightarrow \text{SEI films} \quad (7)$$

Where M=Ni; Co; Mn. $0<x<1$; $0<z<0.04$; $0<y, q, r<x$; $0<n<6$; $0<m<1$.

Figure S16. Schematics of reaction mechanisms for the KNCMF@rGO electrode during the discharging/charging processes under the first two cycles (a); Crystalline structure information of Ni, Co, Mn, NiF_2, CoF_2, MnF_2, NaF, KF, and Na_2CO_3 phases (b), and reaction equation 1-7 (c).

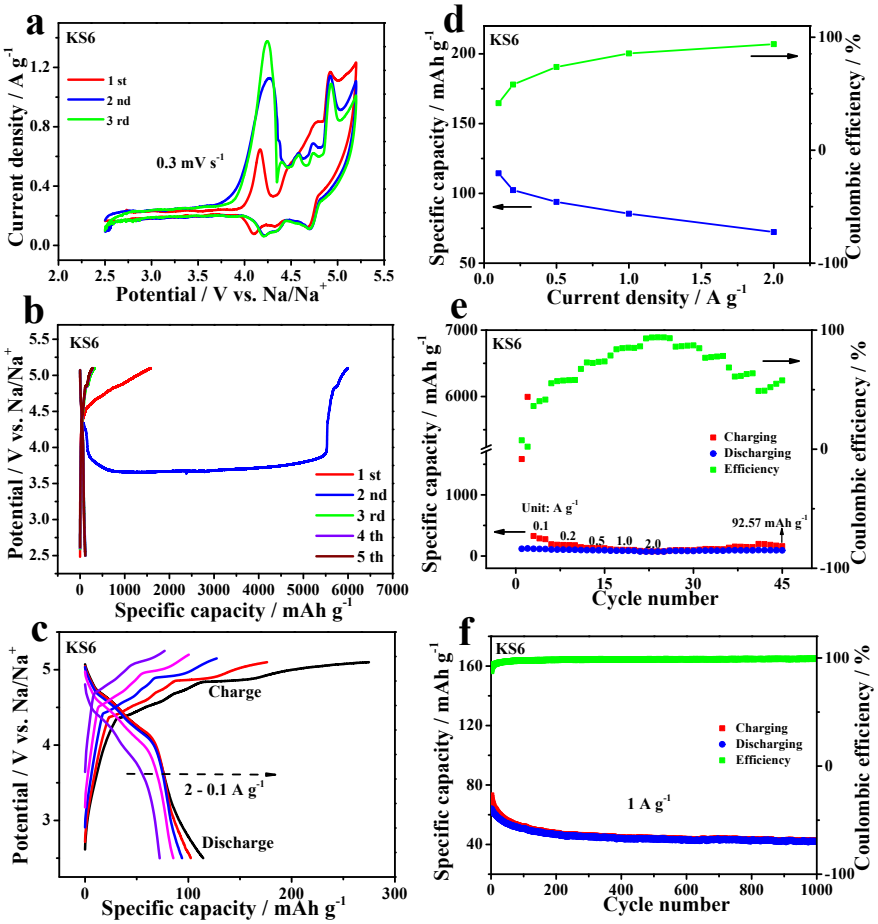

Figure S17. Performance of the KS6 electrode: CV plots for the first three cycles at 0.3 mV s^{-1} (a), GCD curves for the first five cycles at 0.1 A g^{-1} (b), GCD curves at 0.1-2.0 A g^{-1} (c), specific capacity/rate capability and coulombic efficiency at 0.1-2.0 A g^{-1} (d)(e) and cycling behavior at 1 A g^{-1} (f).

Figure S17a-f illustrate the performance of the KS6 electrode. **Figure S17**a-c show the CV plots for the first three cycles at 0.3 mV s^{-1} (a), GCD curves for the first five cycles at 0.1 A g^{-1}(b) and GCD curves for the 5 th cycle at 0.1-2.0 A g^{-1}(c), which show more than three pairs of redox peaks and charging/discharging plateaus, indicating the multi-steps co-insertions of PF_6^- anions and solvents in the graphite layers. **Figure S17**d-f show the specific capacity, rate capability and cycling behavior, which exhibit the specific capacity values of 114.4-72.3 mAh g^{-1} at 0.1-2.0 A g^{-1} and 66 % retention for 1000 cycles at 1 A g^{-1} (**Table S4**). Such an excellent performance of KS6 can be a good positive electrode material used in Na-DIBs and will contribute to the advanced performance of the KNCMF@rGO//KS6 Na-DIBs.

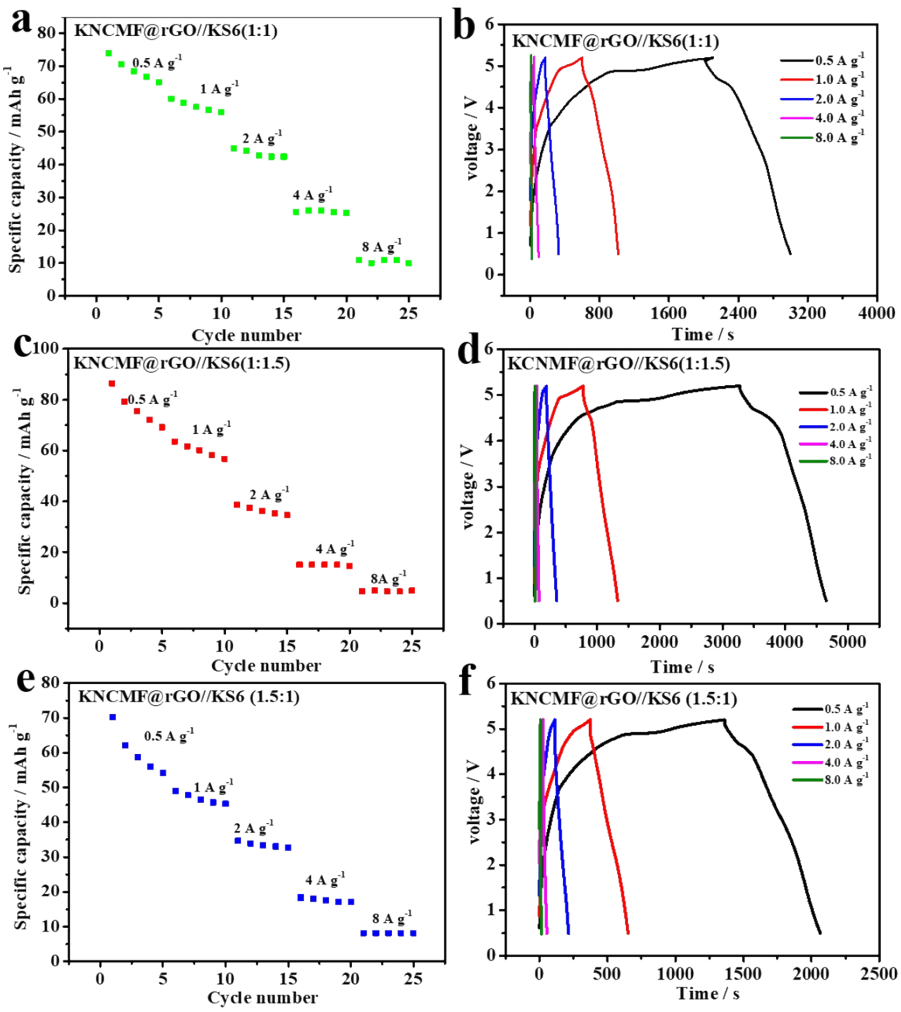

Figure S18. Specific capacity at 0.5-8 A g^{-1} (a) (c) (e), GCD curves at 0.5-8.0 A g^{-1} (b) (d) (f) of the KNCMF@rGO//KS6(1:1/1:.5/1.5:1) Na-DIBs.

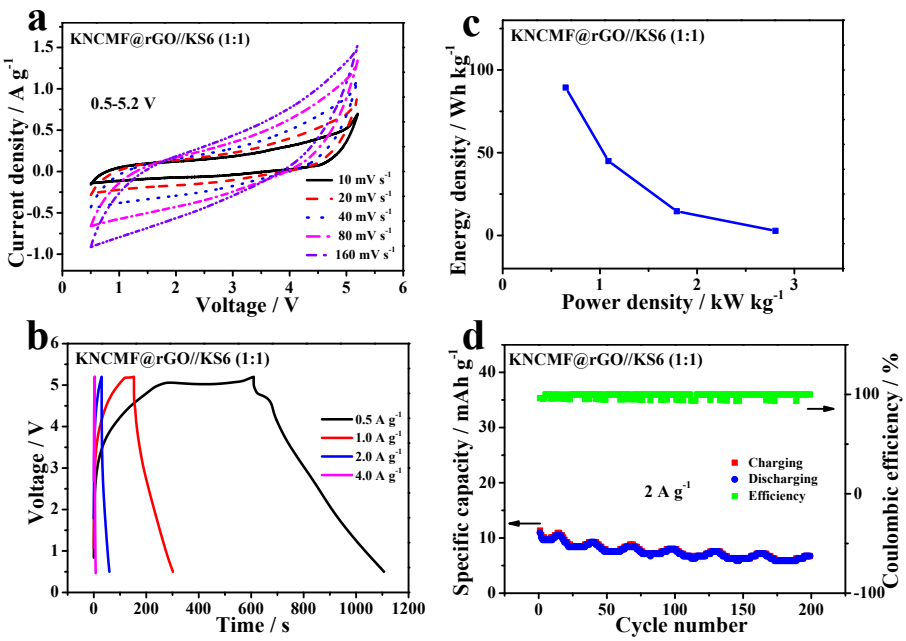

Figure S19. Performance of the Na-DIBs (KNCMF@rGO//KS6) under low (-20 ℃) temperature: CV plots at 10-160 mV s^{-1} (a), GCD curves at 0.5-4.0 A g^{-1} (b), Ragone plots (c) and cycling behavior (d).

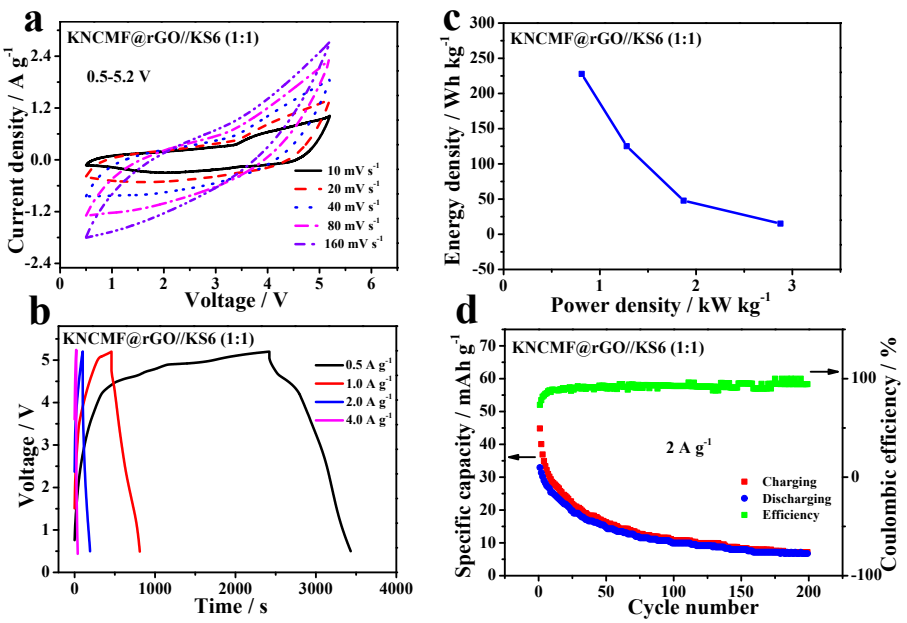

Figure S20. Performance of the Na-DIBs (KNCMF@rGO//KS6) under high (40 ℃) temperature: CV plots at 10-160 mV s^{-1} (a), GCD curves at 0.5-4.0 A g^{-1} (b), Ragone plots (c) and cycling behavior (d).

Table S1. Materials, chemicals, and reagents used in this study.

Materials, chemicals and reagents	Type	Company	Characteristics
$NiCl_2$•6H_2O	AR	SinoPharm	Purity≥98.0%
$CoCl_2$•6H_2O	AR	SinoPharm	Purity≥99.0%
$MnCl_2$•4H_2O	AR	SinoPharm	Purity≥99.0%
KF•2H_2O	AR	SinoPharm	Purity≥99.0%
PVP-K30	GR	SinoPharm	#
EG	AR	SinoPharm	Purity≥99.0%
Graphite	TiMCAL- KS6	TiMCAL	D90: 5.8-7.1 μm; Interlayer distance: 0.3354-0.3360 nm; SSA: 20 $m^2 g^{-1}$; Density-Scott: 0.07 g cm^{-3};
Graphene oxide (GO)	Power	ZhengZhou JingHong New Energy	3-10 floors Conductivity: 2.0*10^5 S m^{-1} SSA: 150~200 $m^2 g^{-1}$
Acetylene black	Battery grade	#	#
Superconductive carbon black	ECP-600 JD	ShenZhen YuLong	Average Diameter: 34nm; SSA: 1400 $m^2 g^{-1}$
NMP	AR	Kermel	Purity≥99.0%
PVDF	Battery grade	#	#
Electrolytes	Na206-181224	MJS	0.85 M $NaPF_6$/EC: EMC: DEC (1:1:1)/5% FEC
Na tablets (Homemade)	Battery grade	#	#
Cu foil	200*0.015	GuangZhou JiaYuan	Total thickness: 15 μm; Weight: 87 g m^{-2}
Carbon coated-Al foil	222*0.015	GuagZhou NaNuo	Total thickness: 17 μm; Strength: 192 Mpa
Glass microfiber filters	GF/D 2.7 μm 1823-025	Whatman	Diameter: 25 mm; Thickness: 675 μm; Weight: 121 g m^{-2}
Cell components	CR-2032	ShenZhen TianChenHe	#

Table S2. Specific capacity and cycling retention of the KNCMF@rGO electrode.

Current density / (A g^{-1})	**Specific capacity of KNCMF@rGO electrode (mAh g^{-1})**
0.02	208.4
0.05	161.8
0.1	128.3
0.2	98.1
0.5	68.3
1.0	43.9
Cycling behavior Retention % / 0.3 A g^{-1} / 500 cycle	66%

Table S3. Specific capacity, rate capability and cycling retention of KNCMF@rGO, KNMF@rGO, KNCF@rGO, KCMF@rGO, KNF@rGO, KCF@rGO and KMF@rGO electrodes.

Current density / (A g^{-1})	**Specific capacity (mAh g^{-1})**						
	KNCMF@rGO	**KNMF@rGO**	**KCMF@rGO**	**KNCF@rGO**	**KNF@rGO**	**KCF@rGO**	**KMF@rGO**
0.02	208.4	250.6	125.3	209.8	238.7	164.0	75.2
0.05	161.8	187.5	95.8	144.7	167.3	135.1	63.5
0.1	128.3	146.1	76.9	112.0	125.0	116.0	54.4
0.2	98.1	117.9	58.6	83.1	93.7	93.1	43.7
0.5	68.3	81.9	39.3	57.2	64.8	67.8	29.6
1	43.9	52.4	27.4	38.2	45.9	49.1	21.0
Rate capability (%)	21.1	20.9	21.9	18.2	19.2	29.9	27.9
Cycling behavior Retention % / 0.5 A g^{-1} / 500 cycle	54.0	94.1	69.5	48.6	30.9	84.9	78.0

Table S4. Specific capacity cycling retention of the KS6 electrode.

Current density / (A g^{-1})	**Specific capacity of KS6 electrode (mAh g^{-1})**
0.1 (2.5-5.1 V)	114.4
0.2 (2.5-5.1 V)	102.3
0.5 (2.5-5.15 V)	93.9
1.0 (2.5-5.2 V)	85.5
2.0 (2.5-5.25 V)	72.3
Cycling behavior Retention % / 1 A g^{-1} / 1000 cycle (2.5-5.2 V)	66%

Table S5. Comparison of electron binding energy of K2p and F1s.

Pristine state	$KNi_{0.1}Co_{0.9}F_3$	$KCo_{0.54}Mn_{0.46}F_3$	$K_{1.1}Zn_{0.17}Mn_{0.83}F_{3.03}$	$K_{0.79}Ni_{0.25}Co_{0.36}Mn_{0.39}F_{2.83}$@rGO
K2p3/2	292.8 eV	293.5 eV	293 eV	295.5 eV
K2p1/2	295.8 eV	296.3 eV	295.8 eV	298.2 eV
F1s	684.5 eV	684 eV	684.5 eV	687.58 eV
Refs.	1	2	3	This work

Table S6. Performance summary of the Na-DIBs in the study under room temperature (25 ℃).

Na-DIBs	Working voltage / V	Energy density / Wh kg^{-1}	Power density / kW kg^{-1}	Cycling behavior / retention %, repeated cycles, current density
KNCMF@rGO//KS6 (1:1)	0.5～5.2	229.64～184.31 114.69～54.22 16.96	0.84～1.59 2.68～4.15 6.1	74%/50/2 A g^{-1} 60%/100/2 A g^{-1} 44%/200/2 A g^{-1} 30%/500/2 A g^{-1}
KNCMF@rGO//KS6 (1:1.5)	0.5～5.2	262.18～177.86 88.67～29.38 7.03	0.68～1.17 1.95～3.08 4.78	50%/50/2 A g^{-1} 40%/100/2 A g^{-1} 33%/200/2 A g^{-1}
KNCMF@rGO//KS6 (1.5:1)	0.5～5.2	190.16～ 130.83 80.72～33.72 12.53	0.97～1.69 2.89～4.63 6.27	61%/50/2 A g^{-1} 47%/100/2 A g^{-1} 37%/200/2 A g^{-1}

Table S7. Performance summary of the Na-DIBs in the study under low (-20 ℃) and high (40 ℃) temperature.

Na-DIBs	Working voltage / V	Temperature (℃)	Energy density/ Wh kg^{-1}	Power density/ kW kg^{-1}	Cycling behavior/ retention %, repeated cycles, current density
KNCMF@rGO //KS6(1:1)	0.5～5.2	-20 ℃	89.38～44.93 14.62～2.81	0.65～1.09 1.79～2.81	69%/50/2 A g^{-1} 73%/100/2 A g^{-1} 62%/200/2 A g^{-1}
KNCMF@rGO //KS6(1:1)	0.5～5.2	40 ℃	227.81～125.08 47.81～15.18	0.81～1.28 1.87～2.88	45%/50/2 A g^{-1} 30%/100/2 A g^{-1} 20%/200/2 A g^{-1}

Table S8. A comparison for the performance of the KNCMF@rGO//KS6 in the study with some reported Na (Li)-DIBs.

Na（Li）-DIBs	Working voltage / V	Energy density / Wh kg^{-1}	Capacity / mAh g^{-1}	Power density/ kW kg^{-1}	Cycling behavior/ retention%, repeated cycles, current density	Refs.
Sn//Graphite (Na-DIBs)	2.0-4.8	144-111	#	0.15-0.793	#	4
MoS_2//Carbon-Graphite (Na-DIBs)	1.0-4.0	#	65（0.1 A g^{-1}）	#	85%/200/0.1 A g^{-1}	5
Si-compound //Graphite (Li-DIBs)	0-3.0	54	#	#	53%/100/0.1 A g^{-1}	6
RGO//Graphite (Li-DIBs)	0-4.0	70	#	1.33	74%/50/1.33 A g^{-1}	7
KNCMF@rGO// KS6 (Na-DIBs)	**0.5-5.2**	**229.64～184.31 114.69～54.22 16.96**	**68.49~57.56 42.86~26.05 10.92 (0.5/1/2/4/8 A g^{-1})**	**0.84～1.59 2.68～4.15 6.1**	**74%/50/2 A g^{-1} 60%/100/2 A g^{-1}**	**This Work**

References

1. Q. L. Xu, R. Ding, W. Shi, D. F. Ying, Y. F. Huang, T. Yan, P. Gao, X. J. Sun and E. H. Liu, *J. Mater. Chem. A*, 2019, 7, 8315-8326.
2. D. F. Ying, R. Ding, Y. F. Huang, W. Shi, Q. L. Xu, C. N. Tan, X. J. Sun, P. Gao and E. H. Liu, *J. Mater. Chem. A*, 2019, 7, 18257-18266.
3. D. F. Ying, Q. L. Xu, R. Ding, Y. F. Huang, T. Yan, Y. X. Huang, C. N. Tan, X. J. Sun, P. Gao and E. H. Liu, *Chem. Eng. J.*, 2020, 388, 124154.
4. M. H. Sheng, F. Zhang, B. F. Ji, X. F. Tong and Y. B. Tang, *Adv. Energy Mater.*, 2017, **7**, 1601963.
5. H. L. Zhu, F. Zhang, J. R. Li and Y. B. Tang, *Small*, 2018, **14**, 1703951.
6. H. Nakano, Y. Sugiyama, T. Morishita, M. J. S. Spencer, I. K. Snook, Y. Kumai, H. Okamoto, *J. Mater. Chem. A*, 2014, **2**, 7588-7592.
7. X. Y. Shi, W. Zhang, J. F. Wang, W. T. Zheng, K. K. Huang, H. B. Zhang, S. H. Feng, H. Chen, *Adv. Energy Mater.*, 2016, **6**, 1601378.